5684 J. Med. Chem. 2010, 53, 5684–5689
DOI: 10.1021/jm100464k

Journal of Medicinal Chemistry Article

Crystal Structure-Based Selective Targeting of the Pyridoxal 5′-Phosphate Dependent Enzyme Kynurenine Aminotransferase II for Cognitive Enhancement†

Franca Rossi,‡ Casazza Valentina,‡ Silvia Garavaglia,‡ Korrapati V. Sathyasaikumar,§ Robert Schwarcz,§ Shin-ichi Kojima,∥ Keisuke Okuwaki,∥ Shin-ichiro Ono,∥ Yasushi Kajii,∥ and Menico Rizzi*,‡

‡DiSCAFF, University of Piemonte Orientale "Amedeo Avogadro", 28100 Novara, Italy, §Maryland Psychiatric Research Center, University of Maryland School of Medicine, Baltimore, Maryland 21228, and ∥Research Division, Mitsubishi Tanabe Pharma Corporation, Aoba-ku, Yokohama 227-0033, Japan

Received April 15, 2010

Fluctuations in the brain levels of the neuromodulator kynurenic acid may control cognitive processes and play a causative role in several catastrophic brain diseases. Elimination of the pyridoxal 5′-phosphate dependent enzyme kynurenine aminotransferase II reduces cerebral kynurenic acid synthesis and has procognitive effects. The present description of the crystal structure of human kynurenine aminotransferase II in complex with its potent and specific primary amine-bearing fluoroquinolone inhibitor (*S*)-(−)-9-(4-aminopiperazin-1-yl)-8-fluoro-3-methyl-6-oxo-2,3-dihydro-6*H*-1-oxa-3a-azaphenalene-5-carboxylic acid (BFF-122) should facilitate the structure-based development of cognition-enhancing drugs. From a medicinal chemistry perspective our results demonstrate that the issue of inhibitor specificity for highly conserved PLP-dependent enzymes could be successfully addressed.

Introduction

Kynurenic acid (KYNA[a]) is a neuroinhibitory metabolite of the kynurenine pathway (KP), the principal mode of tryptophan degradation in mammals.[1] KYNA has several unusual neurobiological characteristics, most remarkably including antagonism of two abundant ionotropic receptors involved in learning and memory, i.e., the α7 nicotinic acetylcholine and the NMDA receptor.[2,3] Since these effects are seen at KYNA concentrations found in the mammalian brain, elevations in brain KYNA might cause cognitive impairments. This mechanism not only may operate under normal physiological conditions but also could play a role in the cognitive deficits seen in catastrophic neurological and psychiatric diseases such as Alzheimer's disease and schizophrenia, both of which present with abnormally high brain KYNA levels.[4,5] In the brain as elsewhere, KYNA is formed enzymatically by the irreversible transamination of the pivotal KP metabolite L-kynurenine (L-KYN) (Scheme 1). This reaction is catalyzed by pyridoxal 5′-phosphate (PLP) dependent aminotransferases by the two-step mechanism described for this class of enzymes.[6] Thus, in the first semireaction, an external aldimine is formed between the C4′ position of the cofactor and the α-amino group of the substrate, L-KYN, which substitutes in Schiff base linkage the ε-amino group of the conserved catalytic lysine. The abstraction of a proton from the substrate Cα produces the quinonoid intermediate that, once reprotonated, yields the corresponding ketimine. The hydration of the iminic double bond by a water molecule leads to the production of a second complex formed by the ketoacid and the enzyme in its pyridoxamine 5′-phosphate-bound form (E·PMP). The details of the irreversible intramolecular condensation of the resulting 4-(2-aminophenyl)-2,4-dioxobutanoic acid intermediate, yielding the final product KYNA, have not been elucidated so far. Finally, the internal aldimine form of the enzyme (E·PLP) is regenerated by the use of a α-ketoacid as the amino group acceptor.

At least four aminotransferases can utilize L-KYN as the amino donor of the transamination reaction in the mammalian brain.[7,8] However, only one of them, kynurenine aminotransferase II (KAT II, E.C. 2.6.1.7), recognizes L-KYN unencumbered by abundant, competing amino acid substrates. This explains why KAT II accounts for the majority of cerebral KYNA synthesis in rat and human brain tissue.[7] Notably, as revealed using mice with a genomic elimination of KAT II, *permanent* reduction in cerebral KAT II activity leads to decreased KYNA formation in vivo and significant cognitive enhancement.[9] Recent studies were designed to probe the functional consequences of an *acute* disruption of cerebral KYNA synthesis using specific KAT II inhibitors. Development of isozyme-specific inhibitors is notoriously difficult, especially in the case of PLP-dependent aminotransferases, since the members of this family share significant conservation of the active site.[10] Early attempts were based on the structure of L-KYN,[11] eventually leading to the synthesis of [(*S*)-4-(ethylsulfonyl)benzoylalanine, *S*-ESBA), which caused a rapid decrease in KYNA formation in the rat forebrain upon intracerebral application.[12] Interestingly, this treatment also promptly raised the extracellular levels of acetylcholine, glutamate, and dopamine, three classic neurotransmitters with well-established procognitive properties.[13−15] Together with

†The atomic coordinates and structure factors have been deposited in the Protein Data Bank (http://www.rcsb.org) with accession code 2xh1.

*To whom correspondence should be addressed. Phone: +39-0321-375712. Fax: +39-0321-375821. E-mail: rizzi@pharm.unipmn.it.

[a] Abbreviations: hKAT II, human kynurenine aminotransferase II; KAT, kynurenine aminotransferase; KYNA, kynurenic acid; L-KYN, L-kynurenine; PLP, pyridoxal 5′-phosphate; PMP, pyridoxamine 5′-phosphate.

 Published on Web 07/19/2010

Scheme 1. Mechanism of the First Half of the Reaction of the Transamination of L-KYN to KYNA Catalyzed by KATs[a]

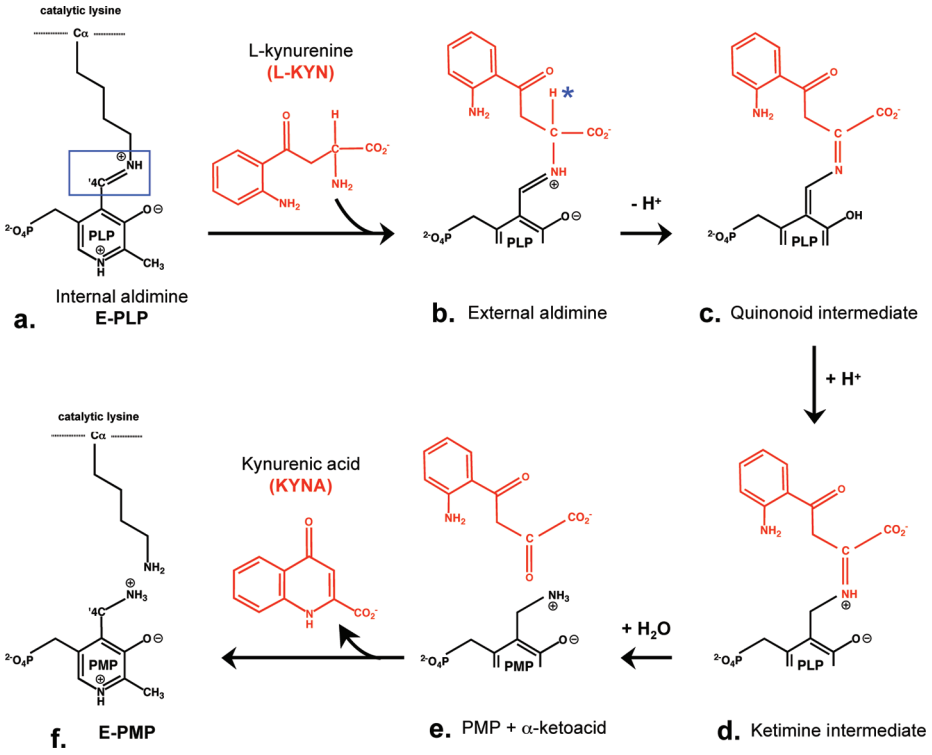

[a] (a) PLP cofactor in the ligand-free form of the enzyme. The Schiff base linkage between the PLP C4′ atom and the catalytic lysine ε-amino group is framed. (b) Transaldimination with the amino acid substrate L-KYN, producing the external aldimine. (c) Abstraction of a proton (labeled by a blue star) from the substrate Cα, producing the quinonoid intermediate. (d) Reprotonation step leading to ketimine formation. (e) Hydrolysis of the ketimine intermediate generating the L-KYN corresponding α-ketoacid [4-(2-aminophenyl)-2,4-dioxobutanoic acid]. The details of the intramolecular condensation of this last molecule to give KYNA are currently unknown. (f) The release of KYNA leaves the enzyme in its PMP form. In the second half of the transamination reaction (not shown), an amino acceptor oxoacid is used to regenerate the PLP-bound form of the enzyme (a) by catalyzing the same set of reverse reactions.

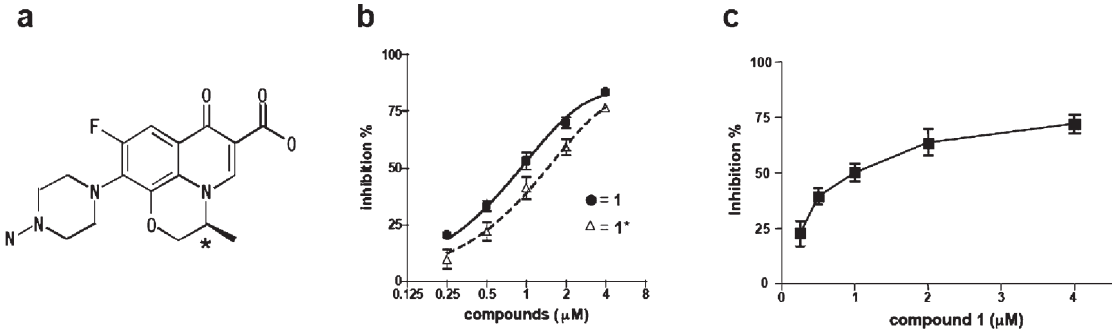

Figure 1. Inhibition of human KAT II by **1**. (a) Chemical structure of **1**. The asymmetric carbon atom is labeled by an asterisk. (b) Both **1** (circles) and its stereoisomer (**1***, triangles) inhibit the activity of recombinant human KAT II in a dose-dependent manner (control activity = 20.4 (nmol/h)/mg protein). Data are the mean of duplicate assays. (c) Inhibition of KAT II by **1** determined in human brain tissue homogenate. Data are the mean ± SEM (control activity = 1.9 ± 0.4 (pmol/h)/mg tissue; $N = 4$).

the demonstration of increased memory function in *S*-ESBA-treated rats [Potter, M. C. Kynurenic Acid, Learning and Memory: The Glutamate Connection. Ph.D. Dissertation, University of Maryland, Baltimore, MD, **2008**], these results validated both the role of KYNA as an endogenous modulator of cognitive processes and the enthusiasm for KAT II as a novel target for procognitive interventions.

Results and Discussion

Characterization of (*S*)-(−)-9-(4-Aminopiperazin-1-yl)-8-fluoro-3-methyl-6-oxo-2,3-dihydro-6*H*-1-oxa-3a-azaphenalene-5-carboxylic Acid (BFF-122) Specific Inhibition of Human KAT II. Although *S*-ESBA can be effectively used to probe KYNA function in the rat brain in vivo, the compound turned out to be a very poor inhibitor of the human orthologue of KAT II (hKAT II), assessed both in brain tissue homogenate and against recombinant hKAT II.[16] By screening an in-house random chemical library on recombinant hKAT II, we recently found that the primary-amine-bearing fluoroquinolone **1** (BFF-122)[17] (Figure 1a), a compound with a structure shared by classic antimicrobial agents,[18] is a potent inhibitor of partially purified rat brain KAT II ($IC_{50} \approx 1\ \mu M$) and can also reduce KYNA synthesis in the rat brain in vivo.[19] In contrast to *S*-ESBA and suggestive of a distinct mechanism of action, however, **1** displayed equally high activity against recombinant hKAT II (IC_{50} = 0.91 and 1.5 μM for the two enantiomers)

Table 1. Data Collection, Processing, and Refinement Statistics[a]

	hKATII·**1**
Data Collection	
space group	$P2_12_12$
cell dimensions	
a, *b*, *c* (Å)	98.32, 152.86, 60.80
α, *β*, *γ* (deg)	90.00, 90.00, 90.00
resolution (Å)	82.76−2.10 (2.21−2.10)
R_{merge}	0.115 (0.398)
$I/\sigma(I)$	5.1 (1.8)
completeness (%)	100.0 (100.0)
redundancy	6.9 (7.0)
Refinement	
resolution (Å)	2.1
no. reflections	53172
R_{work}/R_{free} [b]	19.0/24.5
no. atoms	
protein	6466
ligand/ion	83
water	424
B factors (Å^2)	
protein	28.0
ligand/ion	37.7
water	30.7
rms deviation	
bond length (Å)	0.020
bond angle (deg)	1.812

[a] Values in parentheses are for highest-resolution shell. [b] $R_{work} = \sum|F_o - F_c|/\sum F_o$. $R_{free} = \sum|F_o - F_c|/\sum F_o$, based on 1096 reflections omitted from refinement.

(Figure 1b). Attesting to its pharmacological specificity, **1**, tested in cortical tissue preparations obtained from three to four human donors, was far more potent as an inhibitor of KAT II ($IC_{50} \approx 1\ \mu M$, Figure 1c) than of KAT I (E.C. 2.6.1.64) ($IC_{50} > 30\ \mu M$; control = 0.4 (pmol/h)/mg tissue). In agreement, the IC_{50} of **1** against recombinant hKAT I, too, was $>30\ \mu M$ (control = 7.6 (nmol/h)/mg protein).

To further evaluate the specificity of **1**, we measured the activity of two other human KP enzymes that use L-KYN as their substrate and observed no significant inhibition. Thus, 100 μM **1** inhibited kynurenine 3-monooxygenase activity by 8.3 ± 7.3% (control = 2.1 (pmol/h)/mg tissue) and kynureninase activity by 5.1 ± 2.9% (control = 117.9 (fmol/h)/mg tissue), respectively (averages ± SEM, $P > 0.05$ each, Student's *t* test). It is noted that kynureninase is indeed a PLP-dependent enzyme that does not belong to the aminotransferase family; therefore, **1** emerges as a high specific hKAT II inhibitor with no appreciable activity against other enzymes that use the PLP cofactor as an essential catalytic component.

Crystal Structure of hKAT II in Complex with 1. In order to elucidate the molecular basis of the mechanism of inhibition of hKAT II by **1**, we determined the crystal structure of the enzyme/inhibitor complex (hKAT II·**1**) at 2.1 Å resolution (Table 1). The resulting overall structure consists of a functional dimer (Figure 2) displaying the peculiar swapping of the N-terminal regions (residues 13−46) previously described in the 3D structures of both the ligand-free and L-KYN-bound forms of the enzyme.[20,21]

A close-up view of the active site of the hKAT II·**1** complex (Figure 3a) showed that in each monomer the inhibitor forms an hydrazone adduct with the PLP molecule by establishing a covalent bond that involves the primary amine group of **1** and the C4′ position of the cofactor (Figure 3a and Figure 3b). Since **1** lacks a proton on the N2 atom that occupies a position structurally equivalent to

Figure 2. Molecular architecture of hKAT II in complex with **1**. The two chains forming the functional dimer are colored white and purple. The **1** molecule occupying the active site in both monomers is drawn as sticks and colored yellow.

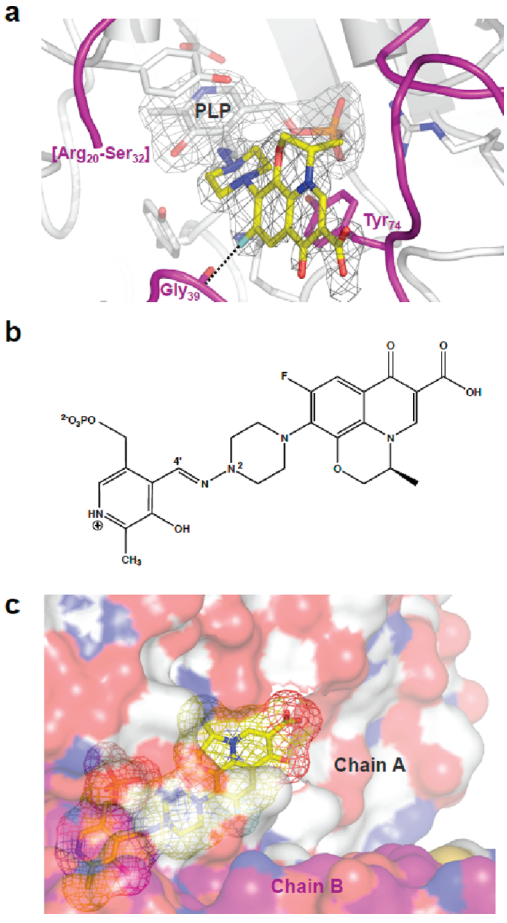

Figure 3. Active site of hKAT II in complex with **1**. (a) Chain A (white) and chain B (purple) of the functional hKAT II dimer are represented as a cartoon. The PLP and compound **1** carbon atoms are depicted as sticks and colored white and yellow, respectively. The portion of the $2F_o - F_c$ electron density map covering the PLP·**1** molecule is shown in gray and contoured at 1σ. Residues providing major interactions to the PLP·**1** complex are drawn as sticks. Protein segment 20−32 has been omitted from the final model. (b) Schematic representation of the PLP·**1** complex shown in (a). (c) Side view of the hKAT II·**1** complex showing the inhibitor carboxylic group exposed to the enzyme surface and highlighting the significant hydrophobic environment (white color) featuring the ligand binding pocket.

the Cα atom of the physiological amino acid substrate, the mandatory proton abstraction step in the transamination process[6] cannot take place, and the enzyme is potently and irreversibly inactivated. In order to verify that **1** behaves as an irreversible hKAT II inhibitor also in solution, we preincubated the enzyme with **1** in a 1:1 molar ratio; after extensive dialysis (Supporting Experimental Section in Supporting Information), hKAT II turned out to be completely inactive. Moreover, we titrated hKAT II in solution with **1** and recorded the corresponding UV−visible spectra (Figure 1 in Supporting Information). Spectroscopic analysis demonstrated that hKAT II reactivity with **1** does not result in the formation of the PMP form of the enzyme, as signaled by the absence of the diagnostic peak around 330 nm, while a **1** concentration dependent increase in the 364 peak was recorded. Finally, by comparing the UV−visible spectra of **1**, free PLP, and a 1:1 mixture of the two molecules, we observed no spectral variation (data not shown), confirming that the covalent adduct does not form in the absence of hKAT II.

The entire PLP·**1** group is firmly anchored at the bottom of the catalytic cavity through a specific and strictly conserved network of contacts that engages the PLP moiety.[20] In turn, the **1** moiety is kept in place by the π-stacking of its heterotricyclic ring to Tyr74 and, on the opposite side, by an electrostatic contact involving the inhibitor fluorine and the carbonyl carbon of Gly39 (Figure 3a). The conformation adopted by the **1** molecule bound to hKAT II revealed that the 3-methyl group does not interact with the protein environment, thus explaining why both **1** stereoisomers act as powerful inhibitors of the enzyme (Figure 1b).

The bulky inhibitor molecule occupies the significantly hydrophobic ligand-binding pocket with the carboxylic group exposed on the enzyme surface (Figure 3c). The observed **1** binding mode interferes with the conformational transition observed in hKAT II along the catalytic cycle that was proposed to control substrate access to the enzyme's active site.[20−23] L-KYN binding triggers a structural rearrangement of the hKAT II N-terminal region (residues 16−32) characterized by a pronounced movement of the loop encompassing residues 16−21 (Figure 4a and Figure 4b). In particular this loop becomes displaced from the ligand binding pocket, changing the enzyme from a closed to an open conformation and allowing Arg20 to engage the bound ligand.[22] In the structure of the hKAT II·**1** complex, no electron density for the majority of such a N-terminal region (residues 20−32; omitted from the final model) is visible, revealing that this structural motif is affected by a significant conformational disorder (Figure 4c). This demonstrates a high conformational plasticity of this N-terminal structural element in hKAT II. In other words, this element not only exists in two alternative conformations, i.e., open and closed, occurring during catalysis, but can be further displaced to accommodate bulkier molecules, such as **1**, in the enzyme's active site (Figure 4d).

Our structural model allows us to explain both the potency and the selectivity of **1** as an inhibitor of hKAT II. While the former can be largely attributed to the formation of a covalent adduct with the PLP cofactor, which permanently inactivates the enzyme, the selectivity of the compound is mainly the result of conformational principles. Indeed, the protein architectures of both hKAT I[24]and mitochondrial aspartate aminotransferase[25] (the third kynurenine aminotransferase present in the brain) are determined by largely preformed ligand binding sites that appear too narrow and rigid to host a bulky molecule such as **1**. This is in contrast to the conformational plasticity of the catalytically important N-terminal motif in hKAT II, which appears to be the key determinant of the observed selectivity of **1**.

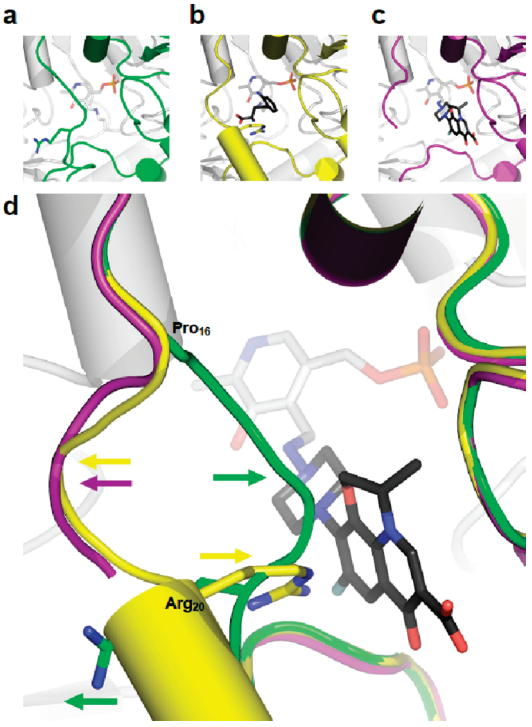

Figure 4. Structural basis of hKAT II inhibition by **1**. The upper images show the active site of hKAT II (a) in its ligand-free form (green, PDB code 2QLR[20]), (b) in complex with L-KYN (yellow, PDB code 2R2N[21]), and (c) in complex with **1** (purple). In (b) and (c), the ligand molecules are colored dark gray. (d) Superposition of the structures of hKAT II shown in (a), (b), and (c). For clarity, only the PLP·**1** molecule and the Arg20 are drawn as sticks. The arrows indicate the direction of the movements of the N-terminal loop and of the Arg20 side chain during catalysis (same color scheme as in (a), (b), and (c)).

From a drug discovery perspective, our data indicate that crucial conformational changes occurring during catalysis can be successfully exploited for developing highly specific inhibitors targeting kynurenine aminotransferases. In this respect, the mechanism of enzyme inhibition by **1** resembles the one reported for the specific human Abl tyrosine kinase inhibitor STI571 (Gleevec/imatinib).[26]

Conclusions

In conclusion, our results demonstrate that the synthesis of specific inhibitors of PLP-dependent enzymes, which has long posed a formidable challenge in drug development, can be successfully achieved. In view of the recently uncovered functional link between brain KYNA and cognitive processes, KAT II appears to be an especially attractive target for exploiting this concept. Thus, it should be possible to use the conformational plasticity of the N-terminal region of the enzyme for structure-based lead optimization to produce novel cognition-enhancing drugs.

Experimental Section

Chemicals. Chemicals used in the experiments were obtained from Sigma-Aldrich (St. Louis, MO). The synthesis, chemical characterization, and purity of **1** have been reported elsewhere.[17] Briefly, the synthetic strategy adopted for the chemical synthesis of **1** followed the one used for quinolones that are readily prepared

starting from a fluoroquinolone core and a nucleophilic amine.[27] The hydrazine can be formed using a two-step procedure, i.e., nitrosylation of the amine with a nitrosylating agent (for example, sodium nitrite in aqueous acidic solution), followed by reduction with zinc (Figure 2 of Supporting Information).

Inhibition Studies Using Recombinant Kynurenine Aminotransferases. Reverse transcription PCR products of human KAT I (A/C X82224.1) and KAT II (A/C AF481738.1) from HEK293 total RNA were cloned into pCR-Blunt II-TOPO (Invitrogen, Carlsbad, CA) and then subcloned into commercially available vectors to produce each recombinant protein fused with maltose-binding protein (MBP) in *E. coli* BL21. The resulting MBP-hKAT I and MBP-hKAT II were purified by conventional methods. Conversion of L-KYN to KYNA was assessed by incubating either 0.2 μg of MBP-hKAT I or 0.1 μg of MBP-hKAT II at 37 °C for 1 h in a total volume of 50 μL of a solution containing 10 μM PLP, 1 mM 2-oxoglutarate, 3 μM L-KYN, and 150 mM Tris-acetate, pH 8.0, in the absence or presence of **1** (30 μM for KAT I and 0.25−4 μM for KAT II). The reaction was terminated by adding trichloroacetic acid at a final concentration of 5%, and de novo produced KYNA was analyzed as described below.

Enzyme Analyses Using Human Brain Tissue Homogenate. Human brain tissues from four individuals [age ± SEM, 40 ± 8 years; average post-mortem interval, 22 ± 5 h] who had died without evidence of neurological or psychiatric disease were obtained from the Maryland Brain Collection (Baltimore, MD). On the day of the assays, samples of the prefrontal cortex (Brodmann area 9, stored at −80 °C) were thawed, homogenized in 5 volumes of ultrapure water, and processed as detailed below. For each tissue homogenate, all assays were performed on the same day. The inhibitory potency of **1** was tested by adding the compound in a small volume immediately before the substrate at the beginning of the respective assay. The final concentration of **1** in the incubation media was up to 100 μM.

Kynurenine 3-Monooxygenase. After dilution of the original homogenate 1:5 (v/v) in 100 mM Tris-HCl buffer (pH 8.1) containing 10 mM KCl and 1 mM EDTA, an amount of 80 μL of the tissue preparation was incubated for 40 min at 37 °C in a solution containing 1 mM NADPH, 3 mM glucose 6-phosphate, 1 U/mL glucose 6-phosphate dehydrogenase, 100 μM L-KYN, 10 mM KCl, and 1 mM EDTA in a total volume of 200 μL. The reaction was stopped by the addition of 50 μL of 6% perchloric acid. Blanks were obtained by including the specific enzyme inhibitor Ro 61-8048 (100 μM, kindly provided by Dr. W. Fröstl, Novartis, Basel, Switzerland) in the incubation solution.[28] After centrifugation (16000*g*, 15 min), a total of 20 μL of the supernatant was applied to a 3 μm HPLC column (HR-80, 80 mm × 4.6 mm, ESA, Chelmsford, MA), using a mobile phase consisting of 1.5% acetonitrile, 0.9% triethylamine, 0.59% phosphoric acid, 0.27 mM EDTA, and 8.9 mM sodium heptane sulfonic acid and a flow rate of 1.0 mL/min. In the eluate, the reaction product 3-hydroxykynurenine was detected electrochemically using a HTEC 500 detector (Eicom Corp., San Diego, CA; oxidation potential, +0.5 V). The retention time of 3-hydroxykynurenine was ∼11 min.

Kynureninase. The original tissue homogenate was incubated in 5 mM Tris-HCl (pH 8.4) containing 10 mM of 2-mercaptoethanol and 50 μM PLP. An amount of 80 μL of the tissue preparation was then incubated for 2 h at 37 °C in a solution containing 90 mM Tris-HCl buffer (pH 8.4) and 100 μM L-KYN in a total volume of 200 μL. The reaction was terminated by adding 50 μL of 6% perchloric acid. To obtain blanks, tissue homogenate was added at the end of the incubation, i.e., immediately prior to the denaturing acid. After centrifugation to remove the precipitate (16000*g*, 15 min), an amount of 25 μL of the resulting supernatant was applied to a 5 μm C_{18} reverse-phase HPLC column (Adsorbosil, 150 mm × 4.6 mm; Grace, Deerfield, IL) using a mobile phase containing 100 mM sodium acetate (pH 5.8) and 1% acetonitrile at a flow rate of 1.0 mL/min. In the eluate, the reaction product, anthranilic acid, was detected fluorimetrically (Perkin-Elmer series 200, Waltham, MA) using an excitation wavelength of 340 nm and an emission wavelength of 410 nm. The retention time of anthranilic acid was ∼7 min.

Kynurenine Aminotransferases I and II (KAT I and KAT II). For the determination of KAT I activity, the original tissue homogenate was diluted (1:1, v/v) in 5 mM Tris-acetate buffer (pH 8.0) containing 10 mM 2-mercaptoethanol and 50 μM PLP and then dialyzed overnight at 4 °C against 4 L of the same buffer to remove competing amino acid substrates. The reaction mixture contained 150 mM Tris-acetate buffer (pH 7.4), 100 μM L-KYN, 1 mM pyruvate, 80 μM PLP, 10 mM L-2- aminoadipic acid (to block KAT II), 10 mM aspartic acid (to block mitochondrial aspartate aminotransferase), and 50 μL of the dialyzed tissue preparation in a total volume of 200 μL. KAT II activity was determined in the original tissue homogenate, which was further diluted (1:1, v/v) in 5 mM Tris-acetate buffer (pH 8.0) containing 10 mM 2-mercaptoethanol and 50 μM PLP. The reaction mixture contained 150 Tris-acetate buffer (pH 7.4), 100 μM L-KYN, 1 mM pyruvate, 80 μM PLP, and 50 μL of the tissue preparation in a total volume of 200 μL. The effects of **1** were compared to those of the specific KAT II inhibitor L-2-aminoadipate (10 mM).

For the measurement of KAT I or KAT II, the reaction mixture was incubated for 2 h at 37 °C, and the reaction was terminated by the addition of 20 μL of 50% (w/v) trichloroacetic acid and 1 mL of 0.1 M HCl. The reaction mixture was then centrifuged to remove proteins (16000*g*, 10 min), and an amount of 20 μL of the supernatant was applied to a 3 μm HPLC column (HR-80, 80 mm × 4.6 mm, ESA), using a mobile phase consisting of 250 mM zinc acetate, 50 mM sodium acetate, 3% acetonitrile and a flow rate of 1.0 mL/min. In the eluate, KYNA was detected fluorimetrically (Perkin-Elmer series 200) using an excitation wavelength of 344 nm and emission wavelength of 398 nm. The retention time of KYNA was ∼7 min.

Crystallization, Data Collection, and Structure Determination. Native crystals of recombinant human KAT II (hKAT II), expressed and purified as described,[20] were obtained by mixing 1 μL of a protein solution at 10 mg/mL with an equal volume of a reservoir solution containing 20% PEG 3350, 0.2 M potassium iodide, and 0.1 M potassium phosphate, pH 8.5, and equilibrating the resulting drop against 500 μL of the reservoir solution at 20 °C. Needle-shaped yellow crystals grew to a maximum dimension of 0.7 mm × 0.2 mm × 0.05 mm in about 3 weeks. The crystals of the hKAT II·**1** complex were obtained by soaking crystals of the PLP form in their crystallization solution with the addition of 0.5 mM **1** for 24 h at 20 °C.

For X-ray diffraction experiments, hKAT II·**1** crystals were directly taken from the crystallization droplet, quickly equilibrated in a solution containing the crystallization buffer and 15% glycerol as the cryoprotectant, and flash-frozen under a liquid nitrogen stream. Diffraction data were collected at 100 K up to 2.1 Å resolution using synchrotron radiation (λ = 0.981 Å) at the ID14 EH1 beamline (European Synchrotron Radiation Facility, Grenoble, France). Data processing was performed with the programs of the CCP4 suite.[29] The structure determination of the hKAT II·**1** complex was carried out by molecular replacement, using the structure of the hKAT II·L-KYN complex (PDB code 2r2n[21]) as the search model where both the ligand and all solvent molecules were omitted. A clear solution was obtained for both cross-rotation and translation functions using the program AmoRe.[30] The initial model was subjected to iterative cycles of crystallographic refinement with the program REFMAC,[31] alternating with graphic sessions for model building using the program O.[32] A random sample containing 1090 reflections was set apart for the calculation of the free *R* factor.[33] The inhibitor molecule was modeled when the *R* factor dropped to a value of around 0.25 at full resolution, based upon both the $2F_o - F_c$ and $F_o - F_c$ electron density maps. Solvent molecules were automatically added with ARP/wARP.[34] The procedure converged to an *R* factor and free *R* factor of 0.19 and 0.24, with

ideal geometry. Data collection, processing, and refinement statistics are provided in Table 1. Figures have been generated with Pymol.[35]

Acknowledgment. We thank Dr Giovanni Battista Giovenzana (University of Piemonte Orientale, Italy) for helpful discussions and the European Synchrotron Radiation Facility (ESFR, Grenoble, France) for data collection at beamline ID14-EH1. This work was supported by grants from Regione Piemonte and MIUR (PRIN 2007 and Interlink 2004) (to M. R.) and by NIH Grant NS25296 (to R.S.).

Supporting Information Available: UV−visible spectra of hKATII titrated with **1** and schematic representation of the preparation of quinolone compounds with a primary amine. This material is available free of charge via the Internet at http://pubs.acs.org.

References

(1) Stone, T. W. Neuropharmacology of quinolinic and kynurenic acids. *Pharmacol. Rev.* **1993**, *45*, 309–379.
(2) MacDonald, J. F.; Jackson, M. F.; Beazely, M. A. Hippocampal long-term synaptic plasticity and signal amplification of NMDA receptors. *Crit. Rev. Neurobiol.* **2006**, *18*, 71–84.
(3) Albuquerque, E. X.; Pereira, E. F.; Alkondon, M.; Rogers, S. W. Mammalian nicotinic acetylcholine receptors: from structure to function. *Physiol. Rev.* **2009**, *89*, 73–120.
(4) Baran, H.; Jellinger, K.; Deecke, L. Kynurenine metabolism in Alzheimer's disease. *J. Neural Transm.* **1999**, *106*, 165–181.
(5) Schwarcz, R.; Rassoulpour, A.; Wu, H. Q.; Medoff, D.; Tamminga, C. A.; Roberts, R. C. Increased cortical kynurenate content in schizophrenia. *Biol. Psychiatry* **2001**, *50*, 521–530.
(6) Eliot, A. C.; Kirsch, J. F. Pyridoxal phosphate enzymes: mechanistic, structural, and evolutionary considerations. *Annu. Rev. Biochem.* **2004**, *73*, 383–415.
(7) Guidetti, P.; Amori, L.; Sapko, M. T.; Okuno, E.; Schwarcz, R. Mitochondrial aspartate aminotransferase: a third kynurenate-producing enzyme in the mammalian brain. *J. Neurochem.* **2007**, *102*, 103–111.
(8) Han, Q.; Robinson, H.; Cai, T.; Tagle, D. A.; Li, J. Biochemical and structural properties of mouse kynurenine aminotransferase III. *Mol. Cell. Biol.* **2009**, *29*, 784–793.
(9) Potter, M. C.; Elmer, G. I.; Bergeron, R.; Albuquerque, E. X.; Guidetti, P.; Wu, H. Q.; Schwarcz, R. Reduction of endogenous kynurenate formation enhances extracellular glutamate, hippocampal plasticity and cognitive behaviour. *Neuropsychopharmacology* **2010**, *35*, 1734–1742.
(10) Amadasi, A.; Bertoldi, M.; Contestabile, R.; Bettati, S.; Cellini, B.; Di Salvo, M. L.; Borri-Voltattorni, C.; Bossa, F.; Mozzarelli, A. Pyridoxal 5′-phosphate enzymes as targets for therapeutic agents. *Curr. Med. Chem.* **2007**, *14*, 1291–1324.
(11) Varasi, M.; Della Torre, A.; Heidempergher, F.; Pevarello, P.; Speciale, C.; Guidetti, P.; Wells., D. R.; Schwarcz, R. Derivatives of kynurenine as inhibitors of rat brain kynurenine aminotransferase. *Eur. J. Med. Chem.* **1996**, *31*, 11–21.
(12) Pellicciari, R; Rizzo, R. C.; Costantino, G; Marinozzi, M; Amori, L; Guidetti, P; Wu, H. Q.; Schwarcz, R. Modulators of the kynurenine pathway of tryptophan metabolism: synthesis and preliminary biological evaluation of (*S*)-4-(ethylsulfonyl)benzoylalanine, a potent and selective kynurenine aminotransferase II (KAT II) inhibitor. *ChemMedChem* **2006**, *1*, 528–531.
(13) Amori, L.; Wu, H. Q.; Marinozzi, M.; Pellicciari, R.; Guidetti, P.; Schwarcz, R. Specific inhibition of kynurenate synthesis enhances extracellular dopamine levels in the rodent striatum. *Neuroscience* **2009**, *159*, 196–203.
(14) Wu, H. Q.; Pereira, E. F.; Bruno, J. P.; Pellicciari, R.; Albuquerque, E. X.; Schwarcz, R. The astrocyte-derived alpha7 nicotinic receptor antagonist kynurenic acid controls extracellular glutamate levels in the prefrontal cortex. *J. Mol. Neurosci.* **2010**, *40*, 204–210.
(15) Zmarowski, A.; Wu, H. Q.; Brooks, J. M.; Potter, M. C.; Pellicciari, R.; Schwarcz, R.; Bruno, J. P. Astrocyte-derived kynurenic acid modulates basal and evoked cortical acetylcholine release. *Eur. J. Neurosci.* **2009**, *29*, 529–538.
(16) Pellicciari, R.; Venturoni, F.; Bellocchi, D.; Carotti, A.; Marinozzi, M.; Macchiarulo, A.; Amori, L.; Schwarcz, R. Sequence variants in kynurenine aminotransferase II (KAT II) orthologs determine different potencies of the inhibitor *S*-ESBA. *ChemMedChem* **2008**, *3*, 1199–1202.
(17) Schwarcz, R.; Kajii, Y.; Ono, S. I. PCT/US2008/083321 (original US patent, US 60/988,231), 2008.
(18) Wolfson, J. S.; Hooper, D. C. Fluoroquinolone antimicrobial agents. *Clin. Microbiol. Rev.* **1989**, *2*, 378–424.
(19) Amori, L.; Guidetti, P.; Pellicciari, R.; Kajii, Y.; Schwarcz, R. On the relationship between the two branches of the kynurenine pathway in the rat brain in vivo. *J. Neurochem.* **2009**, *109*, 316–325.
(20) Rossi, F.; Garavaglia, S.; Montalbano, V.; Walsh, M. A.; Rizzi, M. Crystal structure of human kynurenine aminotransferase II, a drug target for the treatment of schizophrenia. *J. Biol. Chem.* **2008**, *283*, 3559–3566.
(21) Han, Q.; Robinson, H.; Li, J. Crystal structure of human kynurenine aminotransferase II. *J. Biol. Chem.* **2008**, *283*, 3567–3573.
(22) Han, Q.; Cai, T.; Tagle, D. A.; Robinson, H.; Li, J. Substrate specificity and structure of human aminoadipate aminotransferase/kynurenine aminotransferase II. *Biosci. Rep.* **2008**, *28*, 205–215.
(23) Rossi, F.; Schwarcz, R.; Rizzi, M. Curiosity to kill the KAT (kynurenine aminotransferase): structural insights into brain kynurenic acid synthesis. *Curr. Opin. Struct. Biol.* **2008**, *18*, 748–755.
(24) Rossi, F.; Han, Q.; Li, J.; Rizzi, M. Crystal structure of human kynurenine aminotransferase I. *J. Biol. Chem.* **2004**, *279*, 50214–50220.
(25) Hohenester, E.; Jansonius, J. N. Crystalline mitochondrial aspartate aminotransferase exists in only two conformations. *J. Mol. Biol.* **1994**, *236*, 963–968.
(26) Hubbard, S. R. Protein tyrosine kinases: autoregulation and small-molecule inhibition. *Curr. Opin. Struct. Biol.* **2002**, *12*, 735–741.
(27) Hayakawa, I.; Atarashi, S.; Yokohama, S.; Imamura, M.; Sakano, K.; Furukawa, M. Synthesis and antibacterial activities of optically active ofloxacin. *Antimicrob. Agents Chemother.* **1986**, *29*, 163–164.
(28) Rover, S.; Cesura, A. M.; Huguenin, P.; Kettler, R.; Szente, A. Synthesis and biochemical evaluation of *N*-(4-phenylthiazol-2-yl)benzenesulfonamides as high-affinity inhibitors of kynurenine 3-hydroxylase. *J. Med. Chem.* **1997**, *40*, 4378–4385.
(29) The CCP4 suite: programs for protein crystallography. *Acta Crystallogr., Sect. D: Biol. Crystallogr.* **1994**, *50*, 760−763.
(30) Navaza, J. AMoRe: an automated package for molecular replacement. *Acta Crystallogr. A* **1994**, *50*, 157–163.
(31) Murshudov, G. N.; Vagin, A. A.; Dodson, E. J. Refinement of macromolecular structures by the maximum-likelihood method. *Acta Crystallogr., Sect. D: Biol. Crystallogr.* **1997**, *53*, 240–255.
(32) Jones, T. A.; Zou, J. Y.; Cowan, S. W.; Kjeldgaard, M. Improved methods for building protein models in electron density maps and the location of errors in these models. *Acta Crystallogr. A* **1991**, *47*, 110–119.
(33) Brunger, A. T. Assessment of phase accuracy by cross validation: the free *R* value. Methods and applications. *Acta Crystallogr., Sect. D: Biol. Crystallogr.* **1993**, *49*, 24–36.
(34) Perrakis, A.; Morris, R.; Lamzin, V. S. Automated protein model building combined with iterative structure refinement. *Nat. Struct. Biol.* **1999**, *6*, 458–463.
(35) DeLano, W. L. *The PyMOL Molecular Graphics System*; DeLano Scientific: Palo Alto, CA, 2002; http://www.pymol.org.